Computer-Assisted Quantification of Axo-Somatic Boutons at the Cell Membrane of Motoneurons

Thomas M. Lehmann*, *Member, IEEE*, Jörg Bredno, Volker Metzler, *Student Member, IEEE*, Gary Brook, and Wilhelm Nacimiento

***Abstract*—This paper presents a system for computer-assisted quantification of axo-somatic boutons at motoneuron cell-surface membranes. Different immunohistochemical stains can be used to prepare tissue of the spinal cord. Based on micrographs displaying single neurons, a finite element balloon model has been applied to determine the exact location of the cell membrane. A synaptic profile is extracted next to the cell membrane and normalized with reference to the intracellular brightness. Furthermore, a manually selected reference cell is used to normalize settings of the microscope as well as variations in histochemical processing for each stain. Thereafter, staining, homogeneity, and allocation of boutons are determined automatically from the synaptic profiles. The system is evaluated by applying the coefficient of variation (C_v) to repeated measurements of a quantity. Based on 1856 motoneuronal images acquired from four animals with three stains, 93% of the images are analyzed correctly. The others were rejected, based on process protocols. Using only rabbit anti-synaptophysin as primary antibody, the correctness increases above 96%. C_v values are below 3%, 5%, and 6% for all measures with respect to stochastic optimization, cell positioning, and a large range of microscope settings, respectively. A sample size of about 100 is required to validate a significant reduction of staining in motoneurons below a hemi-section (Wilcoxon rank-sum test, $\alpha = 0.05$, $\beta = 0.9$). Our system yields statistically robust results from light micrographs. In future, it is hoped that this system will substitute for the expensive and time-consuming analysis of spinal cord injury at the ultra-structural level, such as by manual interpretation of nonoverlapping electron micrographs.**

***Index Terms*—Active contour, balloon model, computer-assisted microscopy, quantitative microscopy, synaptic profile.**

I. Introduction

TRAUMATIC injury to the human spinal cord induces a complex pattern of functional alterations. Deficits may range from minor motor and sensor disturbances to complete plegia with a variable degree of spasticity [1]. So far, the pathophysiological mechanisms underlying these acute and chronic alterations are only partially understood [2]. Data obtained from animal models suggest that structural alterations of intact neuronal systems below the lesion (e.g., synaptic plasticity) may contribute to altered motoneuron function [3]–[5].

A comprehensive test of this hypothesis requires the employment of an objective, unbiased approach to the quantification of synaptic input to the somal surface of motoneurons. Usually, such investigations are based on a small number of neurons at the ultra-structural level, such as nonoverlapping electron micrographs [6]. However, a system determining the reproducible quantification of axo-somatic boutons at motoneural cell-surface membranes at the light-microscopic level would allow the processing of many more cells compared to the ultra-structural studies and hence, facilitates the achievement of statistically robust results.

Quantitative methods for computer-assisted morphometry and cytometry have already been established during the past decade [7], [8]. It is commonly recognized that precise detection of cytological objects embedded in different morphological structures is the key problem in automatic processing of histological samples by means of digital image analysis [9]. In early approaches, only the number of similar structures, such as cells, was determined [10]. Such recognition of cytological structures in micrographs is tackled mostly by specially enhanced and adapted local thresholding and filtering techniques [11], [12]. A number of systems have been evaluated, comparing automated and manual reference counts. However, all cells were only characterized by a binary number describing their presence. Therefore, early approaches in computer-assisted microscopy are of first-order (order: cell detection).

More sophisticated approaches are able to determine characteristic parameters of each cell in the image, such as their brightness, texture, form, shape or fractal dimension. In most cases, the form of cells is determined [12]–[15]. Due to their pixel-oriented concept, cell counters require additional edge completion when extended to form characterization [11], [16]. Also, variants of region growing [17], [18], model-based parametric fitting of elliptical shapes [13], or semi-automatic contour detection [15] are used to accurately extract closed object boundaries. However, beside the quantification of the number of structures, their global characteristic is parameterized. Therefore, such kind of computer-assisted microscopy system has been named the second-order approach (orders: cell detection, form determination). Local errors in shape detection are tolerable by second-order systems, because their effect on the global form parameters is only minor.

In contrast, the determination of size and distribution of axo-somatic boutons at the cell-surface membrane of a mononeuron

Manuscript received June 20, 2000; revised January 13, 2001. This work was supported in part by the Alfred Krupp von Bohlen und Halbach Stiftung and the Studienstiftung des deutschen Volkes (German Scholarship Foundation). *Asterisk indicates corresponding author.*

*T. M. Lehmann is with the Institute of Medical Informatics, Aachen University of Technology (RWTH), D-52057 Aachen, Germany (e-mail: lehmann@computer.org).

J. Bredno is with the Institute of Medical Informatics, RWTH Aachen, Germany.

V. Metzler is with the Institute for Signal Processing, Medical University of Lübeck, 23569 Lübeck, Germany.

G. Brook and W. Nacimiento are with the Clinic of Neurology, RWTH Aachen, Germany.

Publisher Item Identifier S 0018-9294(01)04167-2.

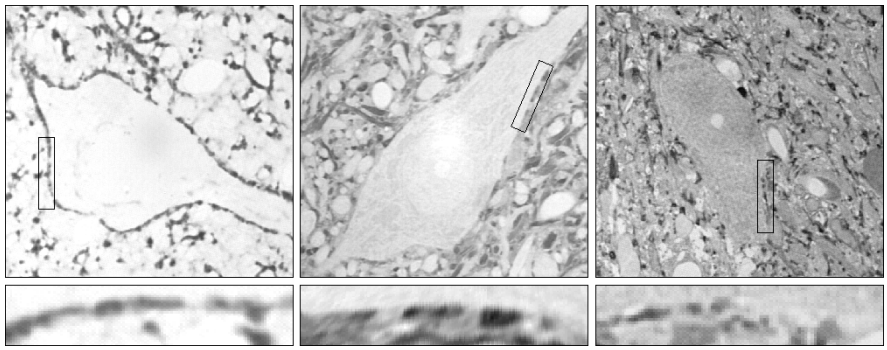

(a) (b) (c)

Fig. 1. The immunohistochemical stains (a) synaptophysin, (b) glycine, and (c) GABA are applied to mark neurotransmitters. To exemplify axo-somatic boutons at the cell membrane, the marked region is magnified below. Note that each image contains a single cell only.

requires high local accuracy. The entire cell shape has to be located exactly to enable detailed measurements along the cell membrane. If parts of the shape cannot be detected validly, they have to be excluded from further image analysis. Therefore, the quantification of axo-somatic boutons at cell membranes in light-microscopic images is of third-order (orders: cell detection, form determination, profile quantification).

Computer-assisted microscopy, addressing third-order image analysis is rather seldom reported. Furthermore, a gold standard for the validation of such systems does not exist. In our case, the true number and size of boutons is neither known nor countable *a priori* by a human observer. For these reasons, the goal of this paper is two-fold. In the first part, a novel system for automated quantification of axo-somatic boutons in micrographs is introduced. The system is capable of measuring the intensity and distribution of immunoreactivity with minimal user interaction for large cell populations and numerous stains by several normalized and absolute measures. The second part of this paper addresses the validation of our approach. Based on numerous micrographs, we have analyzed basic system properties, such as linearity, time-, and shift-invariance. The coefficient of variation of the measures is used to assess their reliability [7]. The sample size required for further experimental use of the method has also been determined.

II. Staining Techniques and Image Acquisition

Adult female Sprague–Dawley rats (200–250 g) were anaesthetized with an intra-peritoneal injection of chloral hydrate (400 mg/kg body weight). The animals were flushed with approximately 100 ml 0.1 M phosphate buffered saline (PBS, pH 7.4) followed by 500 ml 1% paraformaldehyde/2.5% glutaraldehyde in 0.1 M PBS. The spinal cord was dissected and post-fixed in the same fixative for 2 h. Segmental level L4 was removed, washed for 1 h in PBS, post-fixed in osmium tetroxide (1% in 0.1 M PBS) for 1 h, washed and slowly dehydrated with ascending concentrations of ethanol and embedded in a mixture of Epon and Araldite. Following polymerization of the embedding mixture (48 hours at 56°C), tissue blocks were trimmed and serial semi-thin (1 μm) transverse sections were collected onto adjacent slides.

The sections were processed for immunohistochemistry using the peroxidase–antiperoxidase (PAP) method. All sections were etched in a solution of 5% sodium ethoxide (4 minutes) and subsequently washed several times in absolute ethanol. Endogenous peroxidases and nonspecific antibody binding were blocked by incubating sections in 5% H_2O_2 in PBS (5 minutes) followed by 20% normal goat serum in PBS (20 minutes). The primary antibodies used in this investigation were:

1) polyclonal rabbit anti-synaptophysin (Dako, diluted 1 : 500)
2) rabbit anti-glycine (Viva Diagnostika, diluted 1 : 500)
3) rabbit anti-gamma-amino butyric acid (GABA) Viva Diagnostika, diluted 1 : 500.

The sections were incubated in primary antibody for 24 hours at room temperature followed by incubation in goat anti-rabbit IgG for 1 h (Sigma, diluted 1 : 500) and rabbit PAP for 1 hr (Sigma, diluted 1 : 100). The staining was developed by incubating sections for 5 min in 0.5 mg/ml 3,3′-diaminobenzidine containing 0.003% H_2O_2.

All sections were visualized by a Zeiss Axioplan microscope. Sample motoneuronal profiles were captured by a Sony XC-77CE CCD camera controlled by the IPPLUS image analysis system (Media Cybernetics, MD). The images obtained were 512 $\times$ 480 pixels in size with 256 gray levels.

Fig. 1 exemplifies the characteristic appearance of different stains. In each micrograph, only one motoneuron is captured. The cell membrane's region of interest (ROI) partly is magnified below each micrograph. The synaptic boutons marked by the antibodies appear darker than their surrounding. These structures are to be reproducibly quantified by the system.

III. Detection of Cell Membrane and Quantification of Synaptic Profiles

A large number of motoneurons has to be examined. The immunohistochemical stains produce different appearances of cells and axo-somatic boutons. However, every image must be quantified reproducibly regardless of location, size, form or appearance of the membrane, which, for example, may be affected by manual settings of the microscope or histolochemical processing. All steps of image processing have been designed to acknowledge this general requirement.

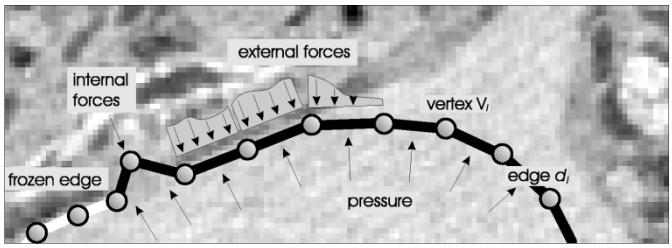

Fig. 2. This figure magnifies a clip of a glycine-stained cell. The balloon is visualized during the iteration by its vertices and edges. A constant pressure from inside expands the balloon. Internal forces are contrary to strong local deformations. External forces are derived from the local gradient in the image to stop the balloon's movement at the cell membrane. Those parts of the membrane are frozen (white edges).

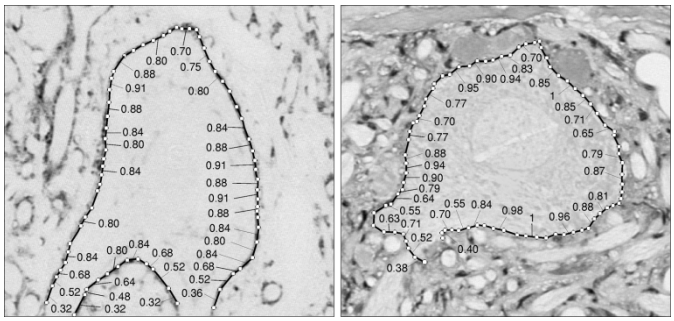

(a) (b)

Fig. 3. The local confidences q_i describe the reliability of the final balloon location. They are attached to the edges $\vec{d}_i$. Note that (a) dendrites and (b) mislocations yield low confidences. For the sake of simplicity, equal q_i are not repeated in the figure.

A. Segmentation of the Cell Body

The segmentation of micrographs must yield the location of the cell membrane, which can vary widely in shape. A closed boundary of the cell body is needed to extract the adjacent cell membrane for quantification. To be useful in an automated system, the detection must be independent of tissue fixation, staining process, and microscope setup.

Active contour models allow detection of arbitrarily shaped objects and result in coherent segmentation. They are used widely to segment medical image material. Based on the original model by KASS *et al.* [19], many variations have been introduced in biomedical engineering [20]. Previously, we have developed a deformable membrane for cell segmentation [21], [22] that is based on the balloon model [23]. This finite element model reflects the properties of biological membranes and enhances their detection [21]. Detailed mathematics of this balloon approach are described elsewhere [22].

Fig. 2 illustrates our membrane model. The balloon consists of I vertices V_i, $i \in \{0, \ldots, I-1\}$ and connecting straight edges $\vec{d}_i$ that form a polygon. An inner pressure iteratively dilates the balloon, which is initialized with a small seed contour inside the cell. In each iteration, the number of vertices is controlled automatically. External forces derived from local gray level gradients affect the edges. Internal forces are derived from mechanical properties and prevent the balloon from forming sharp edges. The balloon is stabilized by freezing those vertices that moved only a little for a number of iterations. This implicitely corresponds to a simulated annealing process, in which the temperature imposing the contour's dynamics is decreased constantly [24]. The frozen contour is enhanced locally by a stochastic technique maximizing the gray level gradient for each vertex [21], [25].

B. Local Confidences

Inhomogeneous illumination and variable staining quality due to tissue properties may cause local detection errors of the cell membrane. A heuristic measure of confidence $q_i \in [0; 1]$ is provided automatically by the algorithm. For each edge $\vec{d}_i$ between V_i and V_{i-1}, q_i results from the product of three factors. Each factor $\in [0, 1]$ gives a fuzzy probability for the edge to represent a part of the actual cell membrane.

1) A cell membrane does not show strong local bends. Therefore, the adjacent angles of the edge $\vec{d}_i$ at V_i and V_{i-1} are checked. The first local confidence factor evaluating the bend of the contour decreases from one down to zero for angles of π down to $2/3\pi$ and below, respectively.
2) The gradient perpendicular to the edge is calculated from the external influences of the balloon model in the last iteration of the segmentation. At a desired transition from unstained to stained areas, the strength of the external force exceeds the inner pressure. Hence, the second local confidence factor evaluating image gradients decreases from one down to zero if external influences are stronger than the pressure or not present, respectively. In other words, local contour positions that are mainly resulting from the internal mechanics of the membrane are labeled with low confidence.
3) Edges near the image border are assumed to belong to a dendrite leaving the image. Since only axo-somatic boutons are to be quantified, the third local confidence factor evaluating the position of the membrane is set to zero or one if the edge is located closer that $1/20$ of the image's size to the border or not, respectively.

Local confidence values are forced to change only moderately along the membrane. Therefore, a moving average filter is applied to improve robustness of the confidence values. In summary, the q_i can be regarded as the probability of correctly detecting the cell membrane, which is assumed to separate different cellular compartments (Fig. 3). They are used as local weights for the quantification of synaptic profiles (see Section III-D).

C. Extraction and Linearization of the Cell Membrane

The balloon's final position is at the inner edge of the motoneural cell-surface membrane. The width of the ROI containing axo-somatic boutons depends on the size of boutons as well as the microscopic magnification, but not on the stain. According to our imaging setup, the width of ROI was set manually to 12 pixels. A two-dimensional (2-D) coordinate transform linearizes the natural curvature of the ROI into a rectangular stripe. In other words, the polygon connecting the vertices V_i is transformed into its parametrization along the curse of curve. The curvature parameter is resampled equidistantly, resulting in the parameter x. The gray levels from

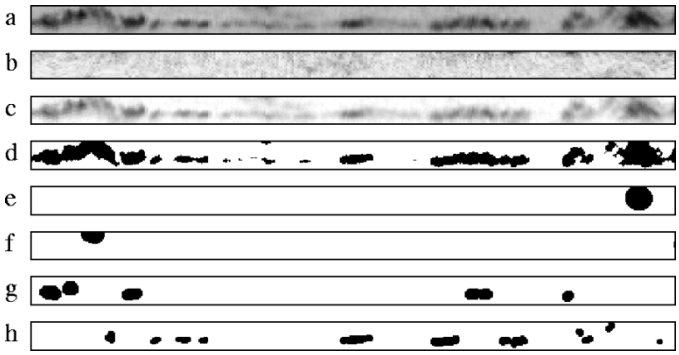

Fig. 4. Extraction and processing of synaptic profiles: (a) initial synaptic profile, (b) reference stripe, (c) normalized profile, (d) binarized profile, and (e)–(h) detected boutons at different scales. Note that profiles (c)–(h) have been inverted for visualization purposes.

the ROI are resampled perpendicular to the curvature by linear interpolation [26]. The resulting rectangular stripe is called the synaptic profile [Fig. 4(a)].

Additionally, an intracellular intensity reference stripe is extracted from the neuronal cytoplasm adjacent to the inner side of the balloon's final location. It is linearized in the same manner as the synaptic profile to determine local illumination inhomogeneities [Fig. 4(b)]. Assuming local continuity of background staining, the synaptic profile is normalized by subtraction from a mean background gray level obtained from the low-pass filtered reference stripe [Fig. 4(c), inverted for visualization].

D. Quantification of Synaptic Profiles

The normalized synaptic profile $M(x, y)$ with length X and height Y represents the staining at the cell-surface membrane, independent of background staining and illumination inhomogeneities [Fig. 4(c)]. It is used to compute quantitative parameters describing comparative measurements for intensity S_{rel} and homogeneity H_{rel} of the staining within the synaptic profile as well as global allocation characteristics $A_{2\text{-D}}$ and $A_{1\text{-D}}$.

1) Staining: The absolute staining S_{abs} of a synaptic profile $M(x, y)$ is defined as its confidence-weighted mean value

$$S_{\mathrm{abs}} = \frac{\sum_{x=0}^{X-1}\sum_{y=0}^{Y-1} M(x,y)\cdot q(x)}{Y\cdot\sum_{x=0}^{X-1} q(x)} \tag{1}$$

where the confidence values q_i are projected into the confidence sequence $q(x)$ according to the coordinate transform of $M(x, y)$. The sequence $q(x)$ decreases irregularities and errors in detection and, hence, improves the robustness of S_{abs}. The normalization to the sum of all $q(x)$ makes S_{abs} independent of the length X of the membrane as well as the correlation of q_i to the staining intensity.

Although $M(x, y)$ was normalized for local illumination inhomogenities, S_{abs} depends on the global illumination intensity of the image, which is a setting of the microscope. To calibrate the system, a physiological reference cell is chosen manually before a series of cells is processed. This reference cell is captured with varying intensities of illumination [Fig. 5(a)]. The illumination level λ is computed as the confident mean gray level of the intracellular intensity reference [Fig. 4(b)]. A third-order polynomial function $S_{\mathrm{ref}}(\lambda)$ is fitted by a least squares approximation [27] to the absolute staining S_{abs}, which are measured at each illumination level λ of the reference cell [Fig. 5(b)].

The staining information S_{rel} provided to the user is a relative measure. It is based on the absolute staining S_{abs} and the illumination level λ of the current cell in comparison to the reference staining $S_{\mathrm{ref}}(\lambda)$

$$S_{\mathrm{rel}} = \frac{S_{\mathrm{abs}} - S_{\mathrm{ref}}(\lambda)}{S_{\mathrm{ref}}(\lambda)}. \tag{2}$$

S_{rel} is an intuitive parameter for the occurrence of staining along the cell membrane. A value of 0% indicates the same amount of staining as in the reference cell. Values $S_{\mathrm{rel}} > 0$ determine higher staining while $S_{\mathrm{rel}} < 0$ describes a decrease compared to the reference cell.

2) Homogeneity: The overall homogeneity of the normalized synaptic profile $M(x, y)$ is assessed by information-theoretic quantities. The entropy

$$H_{\mathrm{abs}} = -\sum_{g=0}^{G-1} p_g \cdot \log_2 p_g \tag{3}$$

introduced by SHANNON quantifies the uncertainty of a probability distribution $P = (p_0, p_1, \ldots, p_{G-1})$ of G outcomes. H_{abs} reaches a maximum if the probabilities p_g are uniform-distributed ($p_g = \mathrm{const.}$) and is zero for a stable state of only a single outcome. In the current context, $G = 256$ outcomes reflect the gray levels $M(x, y) = g$ in the normalized synaptic profile. Once more, the confidence $q(x)$ is applied to increase robustness

$$p_g = \frac{\sum_{x=0}^{X-1}\sum_{y=0}^{Y-1} \begin{cases} q(x) & \forall x, y | M(x,y) = g \\ 0 & \text{else} \end{cases}}{Y\cdot\sum_{x=0}^{X-1} q(x)}. \tag{4}$$

Again, the absolute homogeneity H_{abs} depends on the illumination level λ. Likewise staining S_{rel} in (2), the relative value H_{rel} is obtained from normalization of H_{abs} with the entropy of the reference cell $H_{\mathrm{ref}}(\lambda)$ at illumination level λ. Hence, $H_{\mathrm{rel}} > 0$ indicates that the gray levels are distributed less homogeneously than within the synaptic profile of the reference cell and vice versa.

3) Allocation: Relative measures such as S_{rel} and H_{rel} are applicable only within the same cell line that is based on the same reference. Contrarily, the spatial allocation (2-D allocation) $A_{2\text{-D}}$ measures the absolute coverage of the membrane with boutons

$$A_{2\text{-D}} = \frac{4}{\pi}\cdot\frac{\sum_{x=0}^{X-1}\sum_{y=0}^{Y-1} B(x,y)\cdot q(x)}{Y\cdot\sum_{x=0}^{X-1} q(x)}. \tag{5}$$

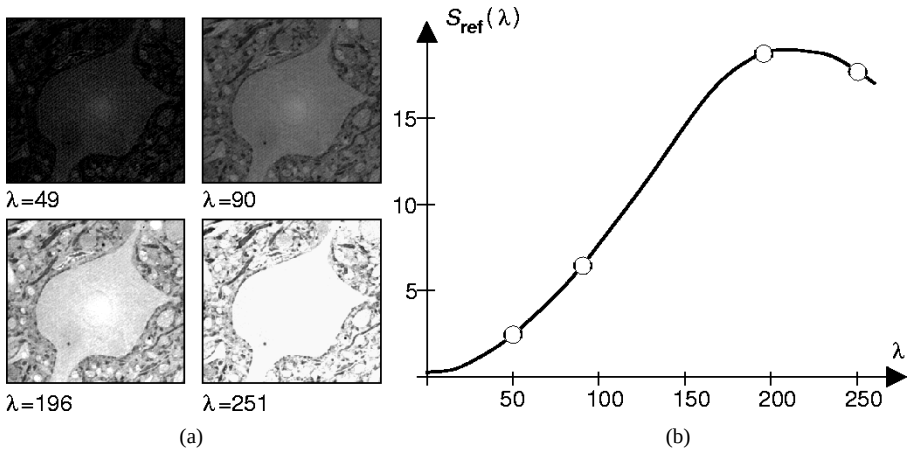

Fig. 5. (a) A reference cell is captured varying the illumination by settings of the microscope. (b) The λ-values are fitted by a third-order polynomial function.

The binarized synaptic profile $B(x, y)$ is computed from $M(x, y)$ by global thresholding [Fig. 4(d)]. Based on a manually selected threshold in one of the reference cell images, the threshold function $T(\lambda)$ is calculated automatically, such that all reference cell images result in the same number of black pixels in $B(x, y)$. The factor $4/\pi$ adapts $A_{2\text{-D}}$ to the natural area of circular objects, such that an allocation of 100% indicates a dense coverage of round-shaped objects in the binary synaptic profile $B(x, y)$.

The projected allocation (1-D allocation) $A_{1\text{-D}}$ measures the occurrence of staining along the membrane. For any x, the projection $B(x)$ of the binary synaptic profile $B(x, y)$ is $B(x) \equiv 1$, if there exists at least one y with $B(x, y) = 1$. Similar to (5), $A_{1\text{-D}}$ is defined as the confident percentage of $B(x)$. Hence, $A_{1\text{-D}}$ specifies the presence of antigen in close proximity to the membrane.

4) Bouton Geometry: The binarized synaptic profile $B(x, y)$ is analyzed further in order to record the geometry of the boutons present. This is done by means of morphological filters [28], which frequently are used in the context of biological image analysis and quantitative cytology [29], [9]. Tophat filters (subtracting the closing [9]) with discs of decreasing radius extract round-shaped objects of different sizes from $B(x, y)$ [Fig. 4(e)–(h)]. Having the width of the ROI defined to 12 pixels, structuring elements with radii of eight, six, four, and two pixel were used. Our morphological filters conform with partially occluded objects. Therefore, disks up to a diameter of 16 pixels can be detected in the ROI of 12 pixels height. The confident amount of set pixels after each filter scale is normalized to the corresponding size of the structuring element. This yields the confident number of discs of a certain size within $B(x, y)$. To enable the comparison of different cells, the measures additionally are normalized with respect to the profile length Y.

E. System Integration and Workflow

The system for synaptic profile extraction and quantification was developed under the software engineering environment Khoros 2 (Khoral Research Inc., Albuquerque, NM). It operates on a Sun Sparc Ultra 2 computer under UNIX (Fig. 6). The user interface is designed to minimize interaction.

1) System Initialization: All image processing is controlled by parameter files that are defined in advance. An expert selects a reference cell for each immunohistochemical stain, captures the cell with at least four illumination settings at the microscope, and transfers the data to the workstation. A reference segmentation of the cell membrane in one of these images is performed manually and the parameter set controlling the balloon is self-determined by the system such that the contour extracted automatically best matches the manual segmentation [30]. Furthermore, the expert selects the global threshold for binarization of the corresponding synaptic profile.

Fig. 7 shows the application for computer-assisted threshold selection. Based on the current threshold, the binarized synaptic profile is transformed in real-time into the image and drawn inside the outlined contour next to the original stained tissue. The detected boutons can easily be compared with the original image contents, which enables simple and reproducible threshold selection.

2) Process Protocol: For each automatically processed cell image, a resulting protocol is printed (Fig. 8). In these protocols, a stained cell and its detected contour are presented next to each other. The gray level of the contour indicates local confidence values, with dark and bright parts assigning high and low detection quality, respectively. Information read from dark parts of the profile has a major influence on the quantification. Based on this visualization, the operator can readily decide whether the contour detection was successful. On the right-hand side of each protocol, staining, homogeneity, and allocation are presented as percentages of the reference cell. For the morphological figures, the radii of the structuring disks are given together with the confident normalization of the number of disks contained in $B(x, y)$. The visualization of these figures by a logarithmically scaled bar chart enables fast user inspection.

3) Workflow: The workflow for a series of slices that already has been initialized is as follows.

- Motoneurons are selected, manually centered, and acquired if the nucleolus is clearly visible. This prevents the same cell to be captured more than once from different histological sections. In addition, this usually yields a perpendicular cut of the cell membrane. The background correction of the microscope is used to remove optical

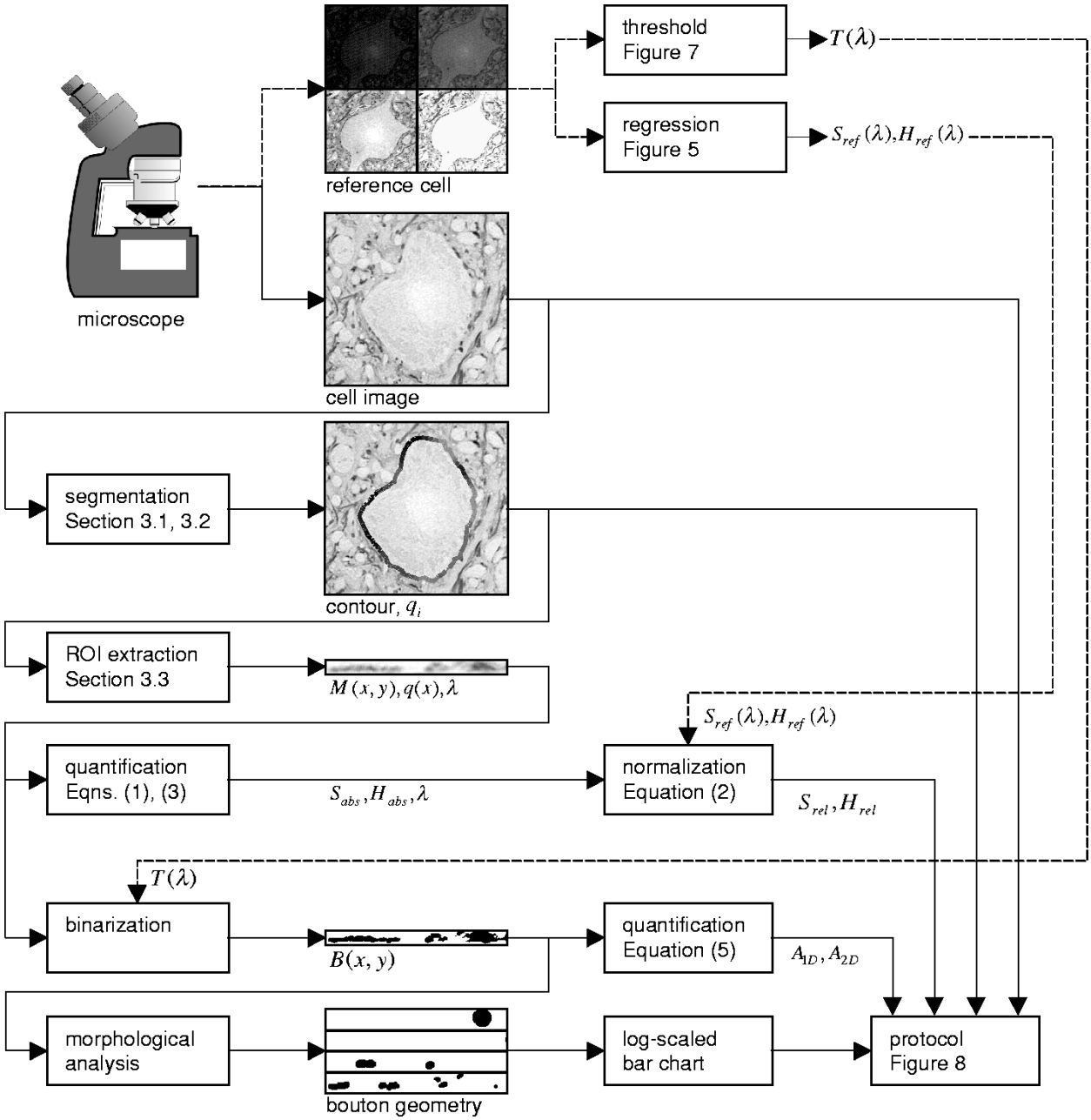

Fig. 6. Process scheme. The dashed lines indicate the manual initialization, which is performed only once. All other steps resulting in the process protocol are performed automatically in batch mode.

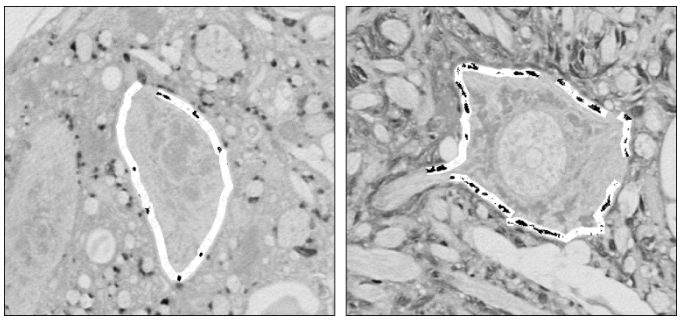

Fig. 7. During manual threshold selection, the binarized synaptic profiles are reprojected in real-time next to the original stained tissue. This figure gives two examples.

artifacts from the image. However, gain and offset remain unchanged for a series of cells in order to minimize user interaction. Therefore, saturation of the charge coupled device (CCD)-chip in bright image areas might occur and has to be handled sufficiently by the algorithm.

- The images are transferred to the workstation and the parameter file is selected accordingly. Thereafter, the system is started and automatically prints the protocol for each processed cell image (Fig. 8). The values are also stored in a database table. The execution is performed in batch mode and takes about 20 seconds per cell.
- The protocols are inspected for local detection errors. Micrographs are rejected and excluded from further evalu-

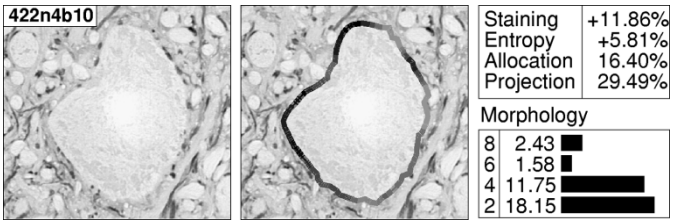

Fig. 8. The process protocol displays the original sample beside the detected contour. Its gray levels indicate the local confidence. The resulting parameters are given on the right.

ation only if local detection errors are labeled with high confidence. By this verification, the physician remains in control of the quantification process, which is important in the medical context of computer-aided diagnosis. However, this control is restricted to the acceptance of contour detection. The user has no ability to modify the quantification values.

- Finally, the database table is exported for use in any application for evaluation, visualization, and/or statistic analysis.

IV. Validation of the Method

The quantification of axo-somatic boutons depends on a precise detection of the cell membrane and a robust correction of influences caused by the imaging system. However, a gold standard to compare with does not exist [31]. Tissue of the spinal cord can be either prepared for electron microscopy at the ultra-structural level or for histological analysis at the light-microscopic level. Hence, the validation of our method was performed stepwise according to the order of our system.

A. Cell Detection

First-order computer-assisted microscopy describes the determination of the number of structures. This can be validated easily because a human observer is able to perform a reference count. In our case, high spatial resolution, which is required for structural analysis of the cell membrane, causes each digital image to display only one cell. Furthermore, manual adjustment during image acquisition always guarantees that the middle pixel of the image is located inside the cell. Therefore, the *a priori* correctness in the first-order stage is 100%. However, our method might be extended easily to analyze more than one cell per image because, at the light-microscopic level, the variance of gray values inside the cell is much lower than outside.

B. Form Determination

The second-order part of our microscopy system automatically locates the cell membrane using a finite element balloon model. Each part of the detected cell membrane is labeled by a local confidence.

From a total of 245 760 image pixels, only about 30 000 are used to build the synaptic profile. Therefore, reliable segmentation is indispensable for quantification. The quality of motoneuronal plasma-membrane detection was tested on 1856 arbitrarily chosen cell images. 31 images were rejected automatically by the system because the overall confidence of the detected cell membrane was too low. In these cases, the balloon either remained completely inside the cell, which was caused by imaging artifacts, or jumped over the cell membrane toward the image borders. The segmentation of the remaining 1825 cells was verified by a neurobiologist (Table I). For all stains, 93% of the cell membranes were detected confidently. The anti-synaptophysin antibody enables the most robust membrane location (correctness $>$ 96%) while the anti-glycine antibody yields only 90% correctly located cell membranes. This correlates to the visual impression from the different stains (Fig. 1).

TABLE I
Detection of Cell Membranes

antibody	# cells	# rejected	correctness
synaptophysin	681	27	96%
GABA	703	67	90%
glycine	441	36	92%
$\sum$	1825	130	93%

C. Bouton Quantification

Cell detection and form determination have been evaluated by a human observer quantitatively and qualitatively, respectively. However, the evaluation of the system's third-order component is not possible by a human observer because neither size nor distribution of axo-somatic boutons can be counted. Therefore, we determined the coefficient of variation C_v to quantify the degree of agreement for repeated measurements of a quantity [7], [32]

$$C_v = \frac{\sigma}{\mu} \tag{6}$$

where μ and σ denote the mean value and standard deviation, respectively. For example, a coefficient of variation $C_v \equiv 0.05$ indicates that 95% of all measurements are located less than $\mu/20$ apart from the mean value σ. In general, $C_v \leq 0.05$ indicates reliable measurements [32].

1) Stochastic Optimization: The quantification of boutons in the synaptic profiles depends on the precise location of the cell membrane that is used to determine the profile. However, the balloon-based segmentation method is based on stochastic optimization. In particular, random shifts of vertices were tested during simulated annealing of the final contour. To determine the system's variation caused by stochastic optimization, an arbitrarily chosen image was analyzed 20 times based on different random seeds. C_v was determined for the absolute staining and homogeneity as well as the spatial and projected allocations (S_{abs}, H_{abs}, $A_{2\text{-D}}$, and $A_{1\text{-D}}$, respectively), which can be computed individually for a single cell (Table II). For all measures, the coefficient of variation was below 3%. Therefore, stochastic optimization of the final balloon position is sufficiently reproducible with respect to the synaptic profile's quantification. In particular, the spatial allocation $A_{2\text{-D}}$ had the highest C_v of 2.78% but the absolute homogeneity H_{abs} varied only less than 1%.

2) Positioning of the Cell: The cells were positioned manually under the microscope before digitization. To determine the variation of quantitative measurements induced by manual placement of the cell, an arbitrarily chosen cell was captured at

TABLE II
VARIATION INDUCED BY STOCHASTIC OPTIMIZATION

	S_{abs}	H_{abs}	A_{2D}	A_{1D}
μ	20.23	5.75	41.74%	76.80%
σ	0.44	0.04	1.16%	1.57%
C_v	2.19%	0.61%	2.78%	2.04%

20 different positions. The specimen was shifted from the center in all eight directions until the cell membrane nearly reached the edge of the image frame. Furthermore, the cell was rotated in steps of approximately 36° until a full rotation was completed. This causes the dendrites to be cut at different positions. Again, the variation was analyzed for S_{abs}, H_{abs}, $A_{\text{2-D}}$, and $A_{\text{1-D}}$ (Table III). The C_v was below 5% for all measures. However, the 2-D allocation was not as robust as the other values. The best reliability was obtained by the absolute homogeneity, which again was below 1%.

3) Settings of the Microscope: The microscope allows manual settings of the focus and the illumination intensity. The computed values strongly depend on the focus setting. The more blurred the image, the less staining is measured. Therefore, the focus has to be adjusted carefully when capturing the images. However, this is done routinely by the neurobiologist because images that are out of focus cannot be inspected manually.

The illumination is adjustable at the microscope without a reliable scale. Our system handles changes of illumination intensity by measuring the illumination level λ. Two equally stained cells were captured by adjusting the light intensity from severe under-exposure to over-exposure, i.e., the saturation of the CCD camera. Fig. 9 shows the dependence of the absolute measures on the illumination level λ. Cell A was used as reference to compute the functional dependence values $S_{\text{ref}}(\lambda)$, $H_{\text{ref}}(\lambda)$, and the threshold $T(\lambda)$. Subsequently, cell B was quantified at different levels of illumination. The coefficient of variation C_v was computed for relative staining and homogeneity as well as spatial and projected allocation (S_{rel}, H_{rel}, $A_{\text{2-D}}$, and $A_{\text{1-D}}$, respectively). If all images of cell B are considered, C_v is up to 11% for $A_{\text{2-D}}$, which is unacceptable. However, within the large range $\lambda \in [25; 230]$, the variation is below 6% for the absolute allocations in two and one dimensions and only about 3% and 2% for the relative measures S_{rel} and H_{rel}, respectively (Table IV).

Although the coefficient of variation depends on the absolute mean when applied to relative measures, Fig. 10 obviously demonstrates the effect of automatic illumination normalization. Note that illumination intensity was identified as the major influence on the resulting gray levels. Brightness changes in the digital image are much weaker when caused by alterations of section thickness and other variations in histological processing. Therefore, the variation of measurements for computer-assisted analysis of synaptic profiles also is negligible.

4) Manual Selection of References: Four observers were asked to choose the threshold for each of ten cells, which were obtained from the same section of the spinal cord, equally stained, and acquired with identical settings of the microscope. Therefore, the ten images yield constant illumination level $\lambda = 232 \pm 0.5$. Each observer selected the threshold, such that the binarized synaptic profile complied with his visual impression (Fig. 7). The coefficient of variation of the chosen threshold

TABLE III
VARIATION INDUCED BY MANUAL PLACEMENT OF THE CELL

	S_{abs}	H_{abs}	A_{2D}	A_{1D}
μ	20.64	5.57	39.49%	73.46%
σ	0.70	0.06	1.96%	2.11%
C_v	3.39%	0.97%	4.96%	2.87%

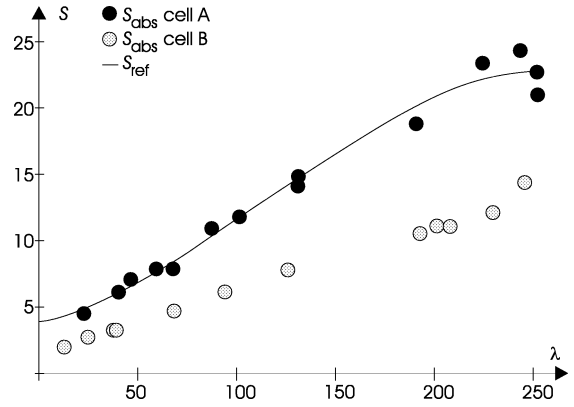

Fig. 9. The absolute staining of two cells was measured on the entire range of illumination levels λ.

TABLE IV
VARIATION INDUCED BY MICROSCOPE SETTINGS

	$S_{\text{rel}} + 100\%$	$H_{\text{rel}} + 100\%$	A_{2D}	A_{1D}
μ	54.49%	83.23%	15.18%	40.85%
σ	1.68%	1.64%	0.83%	2.41%
C_v	3.10%	2.00%	5.50%	5.89%

The variation is based on ten cells. Note that the threshold T is not a direct measure.

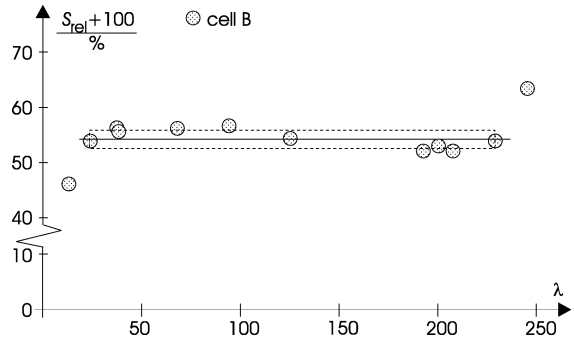

Fig. 10. The relative staining is constant within a large interval of illumination levels λ. The dotted box marks the range for λ yielding $C_v < 3.1\%$.

TABLE V
VARIATION OF THRESHOLD T_i IF CHOSEN BY FOUR OBSERVERS i

	T_1	T_2	T_3	T_4
μ	23.1	28.1	21.0	23.8
σ	3.83	3.75	2.14	2.99
C_v	14.6%	13.3%	10.2%	12.6%

The variation is based on ten cells. Note that the threshold T is not a direct measure.

ranges between 10% and 15% for each of the four observers (Table V). C_v is even larger when computed for each of the ten cells.

However, the threshold T is not a direct measurement by the system. On the one hand, it is obvious that the individual choice of both, the reference cell and the threshold strongly affects spatial and projected allocation measures but not the

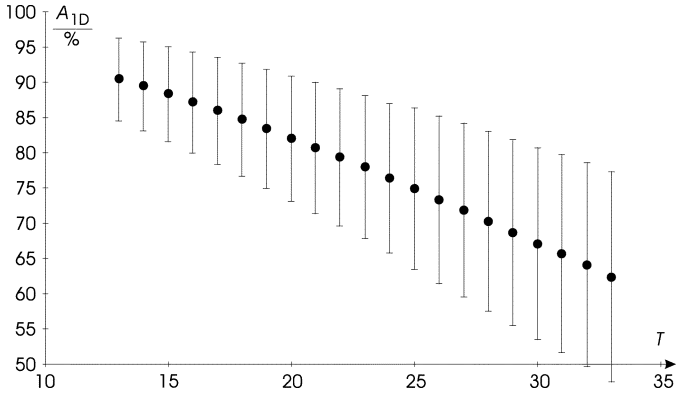

Fig. 11. Dependency of $A_{1\text{-D}}$ from the threshold T, which almost is linear.

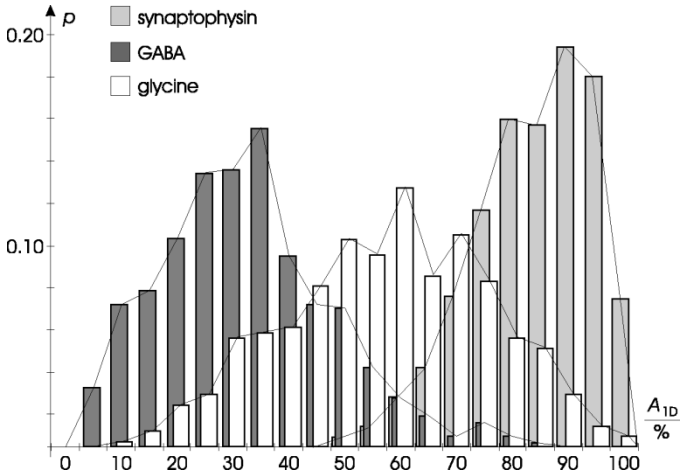

Fig. 12. Histograms of the 1-D allocation $A_{1\text{-D}}$ for different antibodies.

relative staining and homogeneity. On the other hand, any bias or offset in variables is removed when statistical analysis is applied. Hence, only a monotonous progression is required. To evaluate this dependency, $A_{2\text{-D}}$ and $A_{1\text{-D}}$ were calculated for a series of 100 cells identically processed and acquired. In total, 93 synaptic profiles were detected sufficiently. Based on these cells, the allocation measures were computed for different thresholds T. Fig. 11 shows an almost linear dependency $A_{1\text{-D}}(T)$. The curve for $A_{2\text{-D}}(T)$ is similar. On average, if T is increased by one, $A_{2\text{-D}}$ is decreased by 1.6% and $A_{1\text{-D}}$ by 1.35%. The Pearson correlation coefficient r for a linear regression model is 0.999 61 and 0.999 57 for $A_{2\text{-D}}$ and $A_{1\text{-D}}$, respectively. Therefore, the allocation measures are suitable for comparative analysis of different cell series.

V. Preparation for Experimental Applications

In the previous section, we have proven the reliability of our measurement system with respect to variations induced by the system itself. Since we deal with biological objects, a distribution of staining, homogeneity, and allocation is expected when multiple cells which have been processed identically are analyzed. The resulting distribution merges these natural effects with those induced by the system.

The consequences are twofold. Since the system is capable of being adapted to different stains, it is important to analyze which staining technique and measures should be combined for the computer-assisted quantification of axo-somatic boutons at motoneuronal cell body membranes. Furthermore, the determination of sufficient sample sizes is required for statistically valid comparisons of the values obtained.

A. Comparison of Immunohistochemical Stains

The method was used on 1856 cells to specify the distribution for their physiological allocation values using a number of different immunohistochemical stains. Specimen from four animals, processed with three immunohistochemical stains were used to determine spatial and projected allocations. The distribution of $A_{1\text{-D}}$ for synaptophysin, GABA, and glycine is given in Fig. 12. The plots for $A_{2\text{-D}}$ are similar.

Synaptophysin stains all boutons located on the motoneuronal surface and yields the highest allocation for both, $\mu(A_{2\text{-D}}) = 50\%$ and $\mu(A_{1\text{-D}}) = 82\%$. GABA and glycine immunohistochemistry identifies only a subpopulation of these synaptic terminals and hence, the allocation based on these stains is considerably lower (Table VI). Based on synaptophysin, the coefficient of variation C_v ranges between 12% and 25% for $A_{1\text{-D}}$ and $A_{2\text{-D}}$, respectively. Concerning GABA and glycine, C_v increases to greater than 50%. Hence, synaptophysin is identified as the staining method which provides the most mathematically reproducible measurements. However, this method is unspecific and stains all synaptic boutons, whereas GABA and glycine give a more detailed differentiation of synaptic input and permit additional information which facilitates the interpretation of possible functional alterations.

TABLE VI
Variation Induced by Natural Distribution of Biological Measures Determined from Four Animals

	synaptophysin		GABA		glycine	
	A_{2D}	A_{1D}	A_{2D}	A_{1D}	A_{2D}	A_{1D}
μ	50.15%	81.61%	13.16%	29.88%	26.83%	54.83%
σ	12.21%	10.42%	8.09%	15.22%	13.84%	18.18%
C_v	24.3%	12.7%	61.5%	50.9%	51.6%	33.2%

In comparison, the coefficients of variation that are incorporated by the system (Tables II–IV) significantly are smaller.

B. Determination of Sample Sizes

The medical hypothesis motivating this work is that traumatic injury to the human spinal cord causes structural alterations of intact neuronal systems below the lesion. The aim of an oncoming study is to validate a significant reduction of staining in motoneurons below a hemi-section. Therefore, a hemi-section injury was induced in the spinal cord of a rat. A total number of 373 cells stained with synaptophysin were acquired at the light-microscopic level. From these cells, 181 from the operated side below the section and 179 cells from the adjacent un-operated side were accepted for quantification. A total of 13 cells, which equals 3.5%, were rejected.

For S_{rel}, H_{rel}, $A_{2\text{-D}}$, and $A_{1\text{-D}}$, the mean value and standard deviation were computed separately for the two groups. A Wilcoxon rank-sum test with significance level $\alpha = 0.05$ and power $\beta = 0.9$ was assumed to determine the sample size N for each measure (Table VII). Because the standard deviation of both groups varied within an acceptable range, the higher value

TABLE VII
SAMPLE SIZE N REQUIRED FOR EXPERIMENTAL INVESTIGATIONS BASED ON SYNAPTOPHYSIN IMMUNOHISTOCHEMISTRY

	S_{rel}		H_{rel}		A_{2D}		A_{1D}	
	A	B	A	B	A	B	A	B
μ	0	-1.54%	0	-4.60%	38.31%	37.72%	75.22%	70.92%
σ	26.07%	28.51%	9.50%	11.86%	9.18%	9.40%	10.03%	10.57%
N	6344		123		1311		112	

Groups A and B determine the side of the spinal cord below the hemi-section.

was used in each case to obtain a conservative result. The predicted reduction can be validated with 112 cells per group for $A_{1\text{-D}}$ and 123 cells for H_{rel}, respectively. Since each image contains only one cell, an impracticable amount of more than 1000 or 6000 images is needed to validate the reduction of $A_{2\text{-D}}$ or S_{rel}, respectively.

VI. DISCUSSION

We have introduced a system for computer-assisted quantification of synaptic profiles extracted from histochemically stained motoneurons in light micrographs. In comparison to manual investigations at the ultra-structural level, which are expensive and time-consuming, our system facilitates fast, cheap, and mainly automatic achievement of statistically robust results. The method permits objective comparison between different animals and pathological stages. Since the system is structured in a modular way, it can be adapted simply to other staining techniques or cell types and also extended to further tasks, such as quantitative cytology.

Because the appearance of the cells and the staining intensity might vary between different series that were not prepared on the same occasion, a reference cell has to be chosen for each of them. The values S_{rel} and H_{rel} are used to compare cells from the same series, e.g., belonging to different sides of the spinal cord. Here, the reference cell is used only to normalize image brightness but does not affect the comparison of cells. Contrarily, the allocation values $A_{2\text{-D}}$ and $A_{1\text{-D}}$ are used to find a physiological distribution for the coverage of a cell membrane with axo-somatic boutons containing neurotransmitters and, therefore, reliable thresholds must be set for the reference cell in different series. The quantification is characteristic for individual cells and can be computed reproducibly if microscope settings remain unchanged during acquisition of cell series. The variation introduced by the system due to uncertainty in measurement is small compared to the variation of the population.

The system's performance for staining, homogeneity, and allocation was validated by several tests. The morphological analysis of the bouton's shape, which is similar to the pattern spectrum introduced in [33], has not yet been validated. So far, the bar charts printed on the protocols (Fig. 8) are used only to form a visual impression of the occurrence of stained areas with different sizes at the somal surface. In fact, these charts open a 4th-order of computer-assisted microscopy (orders: cell detection, form determination, profile quantification, bouton geometry assessment). They are based on the 2-D allocation, which was shown to be less robust than the projected 1-D allocation.

Therefore, further system standardization is required to yield reliable pattern spectra from synaptic profiles. For example, results will improve if saturation of the CCD camera is avoided. Due to the output charge to voltage transform, its transfer function is currently nonlinear. A calibration procedure, e.g., by use of gray filters, would allow the user to obtain a constant light to voltage coefficient, especially at low intensities of illumination.

The system validation has identified the manual setting of the threshold T to induce the highest variation. Therefore, it limits not only the reliability of 4th-order measures but also the comparison of the projected allocation across a series of cells, which is of third-order. Although it was shown that $A_{1\text{-D}}$ and H_{rel} enable statistically significant investigations with a small sample size, the system generally will be stabilized by automatic threshold selection. Since the synaptic profiles are corrected for local variations of illumination, a nonparametric method for adaptive threshold selection, such as the analysis of cumulative moments of the gray level histogram proposed by Otsu [34], is suitable for further standardization and automatization.

Once initialized manually, the system runs without user interaction. However, images acquired with the microscope must be transferred to the workstation for digital processing, which is done by a few commands. Man–machine interaction is most intensive preparing the parameter files. According to Krief *et al.*, all operations are controlled by a single means of access: namely, a mouse-driven interface [8]. Threshold selection is assisted by real-time visualizing the reprojected synaptic profiles next to the original stained tissue (Fig. 7). The process protocols provide another mean for optimization of man–machine interaction. Large amounts of data can be verified easily based on the protocols (Fig. 8). However, the algorithms are written in C and can be recompiled on more integrated systems for computerized microscopy, e.g., the highly optimized microscope environment [8].

Regardless of technical optimization, the application of our method to neurobiological research will facilitate a better understanding of the pathophysiological mechanisms which underlie the change of function in acute and chronic spinal cord injury. A first challenge is to test the hypothesis that a spinal cord lesion induces a shift in the balance of excitatory and inhibitory synaptic input to motoneurons [35]. A study of the transient reduction of synaptophysin immunoreactive synapses at the somal surface of motoneurons below an experimental spinal cord injury is currently being undertaken. It is expected that such light microscopic investigations of lesion induced changes in excitatory or inhibitory synaptic input will lead to further insights and possible future intervention strategies to improve the clinical situations of patients with spinal cord injury.

ACKNOWLEDGMENT

The authors wish to thank H. Marx for his assistance in performing the micrographs and handling of the digital images this study is based on. The assistance by R. Minkenberg performing statistical analysis is also acknowledged.

REFERENCES

[1] J. Noth, "Trends in pathophysiology and pharmacology of spasticity," *J. Neurol.*, vol. 238, pp. 131–139, 1991.

[2] S. Hochman and D. A. Mc Crea, "Effects of chronic spinalization on ankle extensor motoneurons I–III," *J. Neurophysiol.*, vol. 71, pp. 1452–1490, 1994.

[3] M. E. Helgren and M. E. Goldberger, "The recovery of postural reflexes and locomotion following low thoracic hemisection in adult cats involves compensation by undamaged primary afferent pathways," *Exp. Neurol.*, vol. 123, pp. 17–34, 1993.

[4] H. G. Goshgarian and J. A. Rafolos, "The ultrastructure and synaptic architecture of phrenic motor neurons in the spinal cord of the adult rat," *J. Neurocytol.*, vol. 13, pp. 85–109, 1984.

[5] X. J. Yu and H. G. Goshgarian, "Aging enhances synaptic efficacy in a latent motor pathway following spinal cord hemisection in adult rat," *Exp. Neurol.*, vol. 121, pp. 231–238, 1993.

[6] Q. Tai and H. G. Goshgarian, "Ultrastructural quantitative analysis of glutamatergic and gabaergic synaptic terminals in the phrenic nucleus after spinal cord injury," *J. Comp. Neurol.*, vol. 372, pp. 343–355, 1996.

[7] I. T. Young, "Quantitative microscopy," *IEEE Eng. Med. Biol.*, vol. 15, no. 1, pp. 59–66, 1996.

[8] B. Krief, R. Dye, J. H. Tucker, G. Brugal, and J. M. Chassery, "A new approach to man-machine communication for computerized microscopy," *IEEE Trans. Biomed. Eng.*, vol. 41, pp. 284–286, Mar. 1994.

[9] C. A. Glasbey and G. W. Horgan, *Image Analysis for the Biological Sciences*. Chichester, U.K.: Wiley, 1995.

[10] V. A. Kovalev, A. Y. Grigoriev, H. S. Ahn, and N. K. Myshkin, "Segmentation technique of complex image scene for an automatic blood cell counting system," *Proc. SPIE*, vol. 2710, pp. 805–810, 1996.

[11] K. Wu, D. Gaultier, and M. D. Levine, "Live cell image segmentation," *IEEE Trans. Biomed. Eng.*, vol. 42, pp. 1–12, Jan. 1995.

[12] V. Metzler, T. M. Lehmann, H. Bienert, K. Mottaghy, and K. Spitzer, "Scale-independent shape analysis for quantitative microscopy by mathematical morphology," *Comput. Biol. Med.*, vol. 30, no. 3, pp. 135–151, 2000.

[13] H. S. Wu, J. Barba, and J. Gil, "A parametric fitting algorithm for segmentation of cell images," *IEEE Trans. Biomed. Eng.*, vol. 45, pp. 400–407, Mar. 1998.

[14] V. Metzler, H. Bienert, T. M. Lehmann, K. Mottaghy, and K. Spitzer, "A novel method for quantifying shape deformation applied to biocompatibility testing," *ASAIO Int. J. Artif.Organs*, vol. 45, no. 4, pp. 246–271, 1999.

[15] H. S. Wu and J. Barba, "An efficient semi-automated algorithm for cell contour extraction," *J. Microscopy*, vol. 179, no. 3, pp. 270–276, 1995.

[16] S. H. Ong, X. C. Jin, Jayasooriah, and R. Sinniah, "Image analysis of tissue sections," *Comput. Biol. Med.*, vol. 26, no. 3, pp. 269–279, 1996.

[17] P. Belhomme, A. Elmoataz, P. Herlin, and D. Bloyet, "Generalized region growing operator with optimal scanning: Application to segmentation of breast cancer images," *J. Microscopy*, vol. 186, no. 1, pp. 41–55, 1997.

[18] K. Zheng and M. Kolb, "A particle segmentation method based on nucleation and growth of the background," *J. Microscopy*, vol. 173, no. 2, pp. 165–172, 1994.

[19] M. Kass, A. Witkin, and D. Terzopoulos, "Snakes: Active contour models," *Int. J. Comput. Vis.*, vol. 1, no. 4, pp. 321–331, 1998.

[20] T. Mc Inerney and D. Terzopoulos, "Deformable models in medical image analysis: A survey," *Med. Image Anal.*, vol. 1, pp. 91–108, 1996.

[21] V. Metzler, J. Bredno, T. M. Lehmann, and K. Spitzer, "A deformable membrane for the segmentation of cytological samples," *Proc. SPIE*, vol. 3338, pp. 1246–1257, 1998.

[22] J. Bredno, T. M. Lehmann, and K. Spitzer, "A general finite element model for segmentation in 2, 3, and 4 dimensions," *Proc. SPIE*, vol. 3979, no. 2, pp. 1174–1184, 2000.

[23] L. D. Cohen and I. Cohen, "Finite-element methods for active contour models and balloons for 2-D and 3-D images," *IEEE Trans. Pattern Anal. Machine Intell.*, vol. 15, pp. 1131–1147, Nov. 1993.

[24] D. Rückert, P. Burger, S. M. Forbat, R. D. Mohiaddin, and G. Z. Yang, "Automatic tracking of the aorta in cardiovascular MR images using deformable models," *IEEE Trans. Med. Imag.*, vol. 16, pp. 581–590, Oct. 1997.

[25] G. Storvik, "A Bayesian-approach to dynamic contours trough stochastic sampling and simulated annealing," *IEEE Trans. Pattern Anal. Machine Intell.*, vol. 16, pp. 976–986, Oct. 1994.

[26] T. M. Lehmann, C. Gönner, and K. Spitzer, "Survey: Interpolation methods in medical image processing," *IEEE Trans. Med. Imag.*, vol. 18, pp. 1049–1075, Nov. 1999.

[27] G. H. Golub and C. F. van Loan, *Matrix Computations*. Baltimore, MD: Johns Hopkins Univ., 1989.

[28] R. M. Haralick, S. R. Sternberg, and X. Zhuang, "Image analysis using mathematical morphology," *IEEE Trans. Pattern Analy. Machine Intell.*, vol. 9, pp. 532–550, Apr. 1987.

[29] J. P. Thiran and B. Macq, "Morphological feature extraction for the classification of digital images of cancerous tissues," *IEEE Trans. Biomed. Eng.*, vol. 43, pp. 1011–1020, Oct. 1996.

[30] J. Bredno, T. M. Lehmann, and K. Spitzer, "Automatic parameter setting for balloon models," *Proc. SPIE*, vol. 3979, no. 2, pp. 1185–1194, 2000.

[31] W. Nacimiento, T. Sappok, G. A. Brook, S. Toth, S. W. Schoen, J. Noth, and G. W. Kreutzberg, "Structural changes of anterior horn neurons and their synaptic input caudal to a low thoracic spinal cord hemisection in the adult rat: A light and electron microscopic study," *Acta Neuropathologica*, vol. 90, no. 6, pp. 552–564, 1995.

[32] D. Ingram and R. F. Bloch, *Mathematical Methods in Medicine—Part 1: Statistical and Analytical Techniques*. Chichester, U.K.: Wiley, 1984.

[33] P. Maragos, "Pattern spectrum and multiscale shape representation," *IEEE Trans. Pattern Anal. Machine Intell.*, vol. 11, pp. 701–715, July 1989.

[34] N. Otsu, "A threshold selection method from gray-level histograms," *IEEE Trans. Syst., Man. Cybern.*, vol. 9, no. 1, pp. 62–66, 1979.

[35] J. Destombes, G. Horcholle-Bossavit, and D. Thiesson, "Distribution of glycinergic terminals on lumbar motoneurons of the adult cat: An ultrastructural study," *Brain Res.*, vol. 599, pp. 353–360, 1992.

Thomas M. Lehmann (S'94–M'99) received the masters degree in electrical engineering and the Ph.D. degree (summa cum laude) in computer science from the Aachen University of Technology (RWTH), Aachen, Germany, in 1992 and 1998, respectively.

In 1992, he was Research Scientist at the Faculty of Electrical Engineering, RWTH Aachen. Since 1992, he has been with the Institute of Medical Informatics, Medical Faculty, RWTH Aachen, where he currently heads the Department of Medical Image Processing at the assistant professor level. He co-authored a textbook on image processing for the medical sciences (Springer-Verlag, Berlin, Germany, 1997). His research interests are discrete realizations of continuous image transforms, medical image processing applied to quantitative measurements for computer-assisted diagnoses and content-based image retrieval from large databases.

Dr. Lehmann received the DAGM-Preis '93. The award from the German Association for Pattern Recognition was given for his work on automatic strabometry using Hough transform and covariance filtering. In 1998, he received the Borcher's Medal from the RWTH Aachen for his work on medical image registration. He is Chairman of the German Workshop on Medical Image Processing and Vice-President of the working group Medical Image Processing within the German Society of Medical Informatics, Biometry and Epidemiology (GMDS). He is chairman of the IEEE Joint Chapter Engineering in Medicine and Biology (IEEE German Section). He is member of the International Association of Dentomaxillofacial Radiology (IADMFR) and the Society of Photo-Optical Instrumentation Engineering (SPIE). He serves on the International Editorial Board of Dentomaxillofacial Radiology.

Jörg Bredno received the M.S. degree in mechanical engineering from the Aachen University of Technology. Aachen, Germany, in 1998.

He currently holds a scholarship for his graduate studies at the Institute for Medical Informatics. His research interests include active contour models and quantification of medical images in regard to diagnostic issues He co-authored a textbook on programming of graphical user interfaces.

Mr. Bredno received the Springorum Medal from the Aachen University of Technology in 1999 for his work on ceramic coatings of hip endoprosthesises.

Volker Metzler (S'98) was educated in computing at the Imperial College, London, U.K, and the Aachen University of Technology, Aachen, Germany. He received the M.S. degree from Aachen University of Technology, in 1996.

Until 1998 he had been working on stochastic optimization in image processing and quantitative microscopy with the Medical Faculty of the Aachen University. Currently he is Research Associate with the Institute for Signal Processing of the Medical University of Luebeck, Luebeck, Germany, where he is working in medical image processing. His research interests lie in morphological image processing, scale-space methods, and nonlinear filtering for image restoration, segmentation, and quantitative analysis.

Mr. Metzler is member of the SPIE.

Gary Brook has studied at the University of Aberdeen, Scotland (1978–1982) and was awarded a the degree of B.Sc. (Honors, grade 21) in pharmacology. His post-graduate training was undertaken at the Department of Neuropathology (Head of Department, Prof. L. Duchen) National Hospitals for Nervous Diseases, Queen Square, London, U.K. His studies focused on morphological and electrophysiological investigations of the mechanisms of action of venoms and toxins on nerve and skeletal muscle of the mouse. He received the Ph.D. degree in physiology from the University of London in 1986. Further post-doctoral research was undertaken in London, at the Department of Neuropathology, National Hospitals for Nervous Diseases (1986–1989) and at the Laboratory of Neurobiology, National Institute for Medical Research (glial cell transplantation in the adult mammalian CNS; Head of Department, Dr. G. Raisman, 1989–1994).

Following a move to the Department of Neurology, Aachen University Medical School (Head of Department, Prof. J. Noth, 1994–2000) his research interests have been focused on cellular and molecular consequences of spinal cord injury in man and small laboratory animals. He is currently with the Department of Neuroanatomy, University of Liège, Liège, Belgium (Head of Department, Prof. J. Schoenen).

Wilhelm Nacimiento received the M.D. degree from the University of Heidelberg Medical School, Heidelberg, Germany, in 1987 for experimental investigations on regenerative changes in neurons following transection of their axons. While working toward the M.D. degree, he was being trained in basic neuroscience at the Neurosurgical Research Laboratory at the University of Saarland Medical School, and the Department of Neurobiology at the Max-Planck-Institute, Munich, Germany. From 1987 to 1993, he received his clinical training in Neurology at the Department of Neurology at the Alfried-Krupp Hospital in Essen, and the Aachen Technical University Medical School. In 1993, he ws Board Certified as Clinical Neurologist.

In 1993, he became Staff Physician, and then in 1996 he was awarded the University Docentship in Neurology. In 2000, he became Physician-in-Chief in the Department of Neurology, at the Duisburg Hospital, Duisburg, Germany. His research is focused on the cellular and molecular mechanisms of regeneration and reorganization of the spinal cord following trauma.

Dr. Nacimiento received the Ludwig–Guttmann Prize from the German Society for Paraplegia. He is currently a member of the German Society for Neurology, the German Association for Neurological Intensive Care and the Society for Neuroscience (USA).